Enhanced Proximity Effect in Zigzag-Shaped Majorana Josephson Junctions

Laeven, Tom; Nijholt, Bas; Wimmer, Michael; Akhmerov, Anton R.

DOI
10.1103/PhysRevLett.125.086802

Publication date
2020

Document Version
Final published version

Published in
Physical Review Letters

Enhanced Proximity Effect in Zigzag-Shaped Majorana Josephson Junctions

Tom Laeven,[1,*] Bas Nijholt,[1,†] Michael Wimmer,[1,2,‡] and Anton R. Akhmerov[1,§]
[1]Kavli Institute of Nanoscience, Delft University of Technology, P.O. Box 4056, 2600 GA Delft, Netherlands
[2]QuTech, Delft University of Technology, P.O. Box 4056, 2600 GA Delft, Netherlands

(Received 11 April 2019; revised 10 March 2020; accepted 6 July 2020; published 18 August 2020)

High density superconductor-semiconductor-superconductor junctions have a small induced superconducting gap due to the quasiparticle trajectories with a large momentum parallel to the junction having a very long flight time. Because a large induced gap protects Majorana modes, these long trajectories constrain Majorana devices to a low electron density. We show that a zigzag-shaped geometry eliminates these trajectories, allowing the robust creation of Majorana states with both the induced gap E_{gap} and the Majorana size ξ_M improved by more than an order of magnitude for realistic parameters. In addition to the improved robustness of Majoranas, this new zigzag geometry is insensitive to the geometric details and the device tuning.

DOI: 10.1103/PhysRevLett.125.086802

Introduction.—A hybrid structure containing a semiconductor with strong spin-orbit coupling coupled to a superconductor can become topological upon application of a magnetic field stronger than a critical field B_{crit}, with Majorana bound states appearing on its edges [1,2]. Majorana bound states are a promising candidate for forming the basis of a stable platform for topological quantum computing [3–6]. Much of the experimental effort [7–11] currently focuses on creating pairs of Majorana bound states in hybrid normal-superconductor (NS) nanowire structures.

Recently, a modified setup has been proposed [12,13] relying on a superconductor-normal-superconductor (SNS) junction to lower the critical magnetic field B_{c} by introducing a superconducting phase difference ϕ. When both NS interfaces are transparent, the SNS junction enters the topological phase at $\phi = \pi$ at any finite B field. Two groups [14,15] have realized this system experimentally, but did not yet observe a hard induced superconducting gap.

An important challenge in creating stable Majoranas is the appearance of a soft gap—a power law decay instead of an exponential decay of the density of states near zero energy. In clean systems, a soft gap arises due to the reduction of the induced gap for states with the momentum directed along the junction [16,17]. From a semiclassical perspective, these momenta correspond to long paths through the semiconductor without interruption by the superconductor, shown in Fig. 1(a). These long trajectories have long flight times $\tau_f \approx L_t/v_F$ (see Fig. 1), where L_t is the trajectory length and v_F the electron Fermi velocity. Equivalently, the Thouless energy of these trajectories $E_{\mathrm{TH}} = \hbar/\tau_f$ is small, resulting in a small gap $E_{\mathrm{gap}} \ll \Delta$. This problem does not appear when the Fermi surface is small and the zero point motion dominates the transverse velocity, making a low filling of the bands a possible work around [17,18]. However, tuning the system to a low chemical potential requires a precise knowledge of the band positions and makes the device more sensitive to disorder or microscopic inhomogeneities. On the other hand, disorder scatters these long trajectories and introduces a cutoff on the scale of the mean free path [19–21] which Ref. [22] proposes to use to improve Majorana properties; however, disorder is impossible to control to a required precision experimentally. In the Supplemental Material [23], we compare the size of E_{gap} as a function of the mean free path l_e for zigzag and straight systems at $\phi = 0$ and $\phi = \pi$ and confirm that the zigzag geometry and disorder both increase E_{gap} through a similar mechanism.

We propose a new experimental setup [see Fig. 1(b)] for the creation of Majoranas that eliminates long trajectories and, therefore, prevents the appearance of a soft gap, while also increasing the topological gap (the smallest gap in the dispersion relation) by more than an order of magnitude, depending on the parameters. The setup consists of a zigzag or snakelike geometry for the semiconductor where long trajectories are not possible due to the geometry.

Setup.—We consider a Josephson junction (Fig. 1) consisting of a 2D strip of semiconductor, with superconductors on both sides [12,13]. (In the Supplemental Material [23], we demonstrate that similar physics also occurs in devices with a single superconductor.) We modulate the shape of the normal region to be either zigzag, as depicted [Fig. 1(b)], or a more smooth sinusoidal-like shape. Similar to the straight system [12], we apply a magnetic field B_x along the x axis. The Bogoliubov-de Gennes Hamiltonians H_N and H_{SC} of the normal region and the superconducting (SC) region are

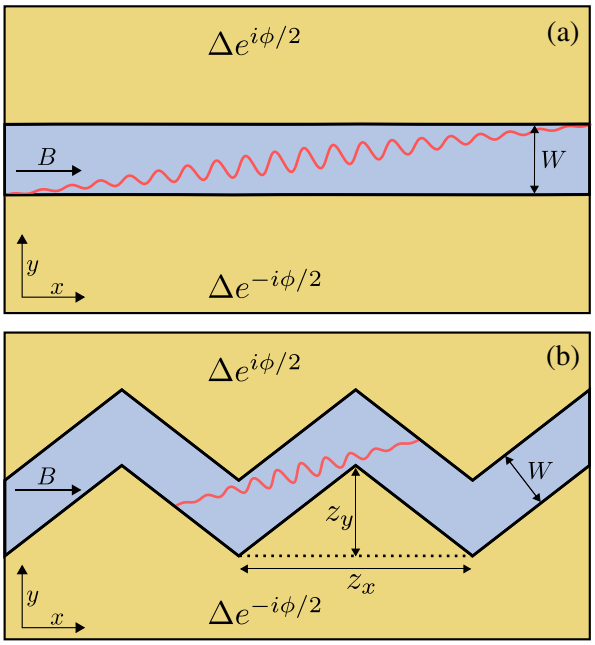

FIG. 1. The straight (a) and the zigzag (b) SNS junction. The zigzag pattern has a peak-to-peak amplitude z_y and a period z_x. The yellow areas are superconductors with a phase difference of ϕ between the top and the bottom. The middle area is the semiconductor of width W. A magnetic field B pointing in the x direction causes a Zeeman splitting in the semiconductor. A trajectory traveling at a grazing angle (red curve) has a very long flight time τ_f and a very small induced gap $E_{gap} \ll \Delta$. At the same time, the zigzag geometry limits the length of a trajectory, therefore, lowering τ_f and increasing E_{gap}.

$$H_N = \left[\frac{\hbar^2(k_x^2+k_y^2)}{2m_{\text{eff}}} - \mu + \alpha(k_y\sigma_x - k_x\sigma_y)\right]\tau_z + E_Z\sigma_x, \tag{1a}$$

$$H_{\text{SC}} = \left[\frac{\hbar^2(k_x^2+k_y^2)}{2m_{\text{eff}}} - \mu\right]\tau_z + \Delta\cos\frac{\phi}{2}\tau_x + \Delta\sin\frac{\phi}{2}\tau_y. \tag{1b}$$

Here, k_x and k_y are the momentum components of the wave vector, μ is the chemical potential, and m_{eff} is the effective electron mass. The strength of the Rashba spin-orbit coupling is α and a Zeeman splitting $E_Z = \frac{1}{2}\mu_B g B_x$. The superconductor has a coupling strength Δ, and the phases of the superconductors are $\pm\phi/2$. The Hamiltonian acts on the spinor wave function $\Psi = (\psi_{e\uparrow}, \psi_{e\downarrow}, \psi_{h\downarrow}, -\psi_{h\uparrow})^T$, where ψ_e, ψ_h are its electron and hole components, and $\psi_\uparrow, \psi_\downarrow$ are the spin-up and spin-down components. The Pauli matrices σ_i act on the spin degree of freedom and τ_i act on the electron-hole degree of freedom. We consider a zigzag pattern with a period z_x, a peak-to-peak amplitude z_y, and W the width of the junction [see Fig. 1(b)]. Later, we relax this assumption and show that the exact shape is unimportant.

We discretize our continuum Hamiltonian [Eq. (1b)] on a square grid and implement a tight-binding model using Kwant [24]. To preferentially sample important regions of parameter space, we use the Adaptive package [25]. The entire source code and the resulting raw data are available in Ref. [26].

Unless noted differently, the Hamiltonian parameters are $\alpha = 20$ meV nm, $g = 26$, $m_{\text{eff}} = 0.02m_e$, $\mu = 10$ meV, $B_x = 1$ T, $\phi = \pi$, and $\Delta = 1$ meV; and the geometry parameters are $W = 200$ nm, the period of the zigzag $z_x = 1300$ nm, the discretization constant $a = 10$ nm, and the lengths of the superconductors $L_{\text{SC}} = 300$ nm. Our results only weakly depend on the material parameters.

Band structures.—We apply sparse diagonalization to the supercell Hamiltonian at different momenta k_x to compute the band structure. Because of the large periodicity of the zigzag and the resulting large supercell, the band structure is heavily folded. In Fig. 2, we show the resulting band structures of zigzag systems with varying z_y. The introduction of the zigzag has a striking effect: the bands flatten out and the topological gap increases by more than an order of magnitude.

In the unfolded band structure of a straight system, shown in Fig. 2(a), the lowest energy states occur at $k \approx k_F$. We interpret the increase of the gap E_{gap} shown in Figs. 2(b) and 2(c) as an effect of the zigzag geometry removing these long trajectories traveling at grazing angles. Besides the increased E_{gap}, the states from different segments of the zigzag pattern have a negligible overlap and, therefore, have a vanishing quasiparticle velocity v. This reduction in velocity strongly reduces the Majorana size, as we discuss in the next section. Finally, in a zigzag geometry, every trajectory encounters a superconductor close to normal incidence. Normal incidence has a higher transmission probability for entering the superconductor and, therefore, a higher Andreev reflection amplitude. This provides another mechanism of the gap enhancement.

Localization lengths and shape effects.—We model a finite system and compute the Majorana wave function in different geometries: ribbon, zigzag, sinelike parallel curves, and a variant of the latter with disordered edges. By diagonalizing the Hamiltonian, we find the Majorana energy E_M, and by using the corresponding eigenstate of that lowest energy, we get the wave function. When determining the Majorana size ξ_M in a zigzag system, we reduce the finite size effects by introducing a particle-hole symmetry breaking potential $V\sigma_0\tau_0$ on one edge, such that one of the Majorana states is pushed away from zero energy. Then, we find ξ_M by fitting an exponential to the density of the single Majorana wave function projected on the x axis. In the straight system, we use the eigenvalue decomposition of the translation operator at zero energy [18] for performance reasons.

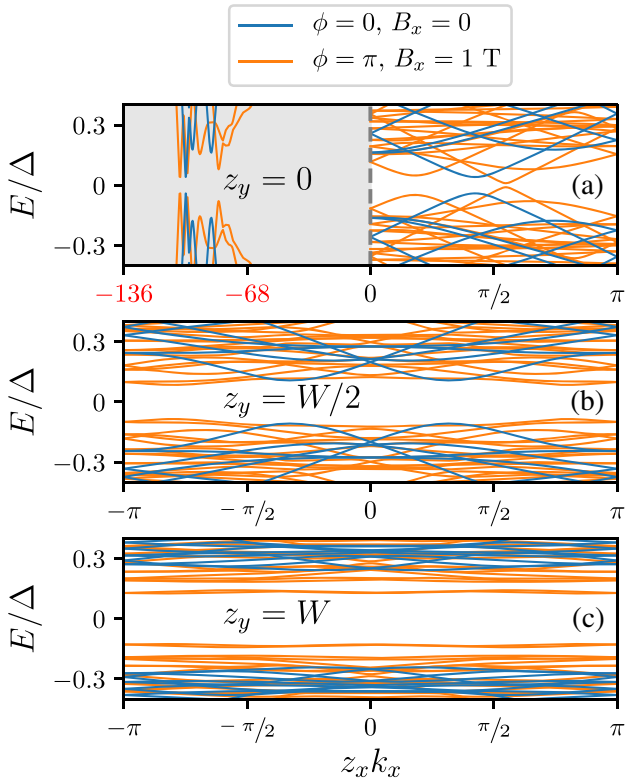

FIG. 2. Band structures of the system in Fig. 1(b) with different zigzag amplitudes. The blue lines correspond to a trivial phase ($\phi = 0$, $B_x = 0$) and the orange lines to a topological phase ($\phi = \pi$, $B_x = 1$ T). The three subplots are for different amplitudes of the zigzag, with (a) a straight system $z_y = 0$, (b) $z_y = W/2$, and (c) $z_y = W$, where $W = 200$ nm is the junction width. Subplot (a) has a different x scale for $k_x < 0$ from the other subplots and displays the unfolded band structure. For the right-hand side of (a) ($k_x > 0$), (b), and (c), the folding is the same, such that the velocity $v = dE/dk$ can be compared visually. Once there are no more straight trajectories inside the junction (when $z_y = W$), the spectrum becomes insensitive to the momentum k_x and equivalently, the quasiparticle velocity v decreases. When the zigzag amplitude increases, the band gap E_{gap} increases by an order of magnitude. The combination of these ensures a significant decrease of the Majorana size $\xi_M \propto v/E_{\text{gap}}$. The parameter values are listed at the end of the Setup section.

We show the resulting Majorana wave function densities $|\psi_M|^2$ in different geometries in Fig. 3 using the same Hamiltonian parameter values. In the straight system [Fig. 3(a)], we see that the decay of the density is long compared to the system size. This is a result of the small topological gap combined with the quasiparticle velocity $v \approx v_F$ yielding a large Majorana size

$$\xi_M = \hbar \frac{v}{E_{\text{gap}}}. \tag{2}$$

This result follows from an avoided crossing shape of the dispersion relation near the Fermi momentum. Therefore,

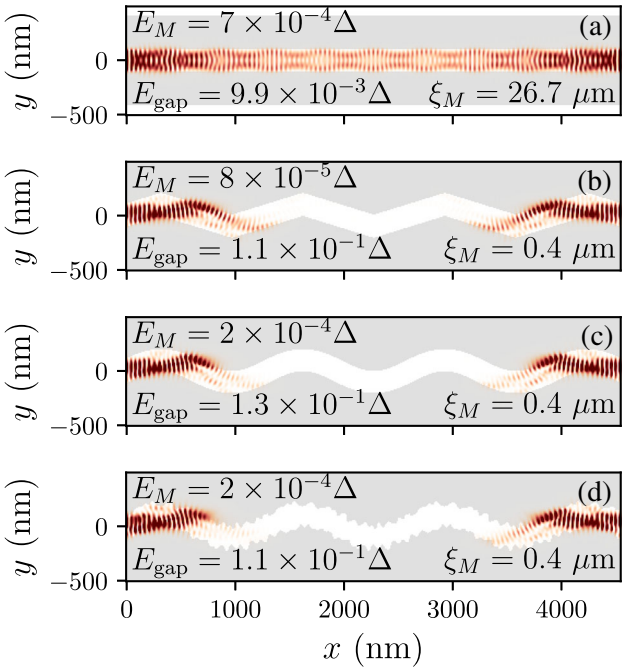

FIG. 3. Density of Majorana wave functions $|\psi_M|^2$ for different geometries. With (a) a straight system, (b) a zigzag system, (c) a system where lines parallel to a sinusoid defines the normal region, and (d) similar to (c) but with disordered edges. Inside the figure, we indicate the Majorana length (or coherence length) ξ_M, the Majorana energy E_M (the energy of the first excited state), and the topological energy gap E_{gap}. We observe that ξ_M for the straight system is almost 2 orders of magnitude longer and E_{gap} more than an order of magnitude smaller than for the zigzag systems. The robustness of E_{gap} and ξ_M across the zigzag geometries means that the details of the geometry do not matter for the improvements to occur. The length of the system is $3.5z_x = 4550$ nm, the remaining parameter values are listed at the end of the Setup section.

in straight junctions, the wave function extends to the center of the system, resulting in highly overlapping Majoranas and a Majorana coupling E_M comparable to E_{gap}.

We observe that, in zigzag systems, the Majorana properties improve independently of specific geometric details. All of the zigzag-type geometries have ξ_M improved by a factor ~70 and have the Majorana wave function localized within one segment of the zigzag. Further, the topological gap E_{gap} is an order of magnitude higher than in the straight junction, and as mentioned in the Band structures section, the quasiparticle velocity v is more than an order of magnitude lower.

Topological phase diagram.—In Fig. 4, we compare the phase diagrams of the straight and the zigzag junctions. We plot E_{gap} as a function of magnetic field and chemical potential [$E_{\text{gap}}(B_x, \mu)$], and of magnetic field and superconducting phase difference [$E_{\text{gap}}(B_x, \phi)$] for both a straight system [4(c) and 4(e)] and a zigzag system [4(d) and 4(f)].

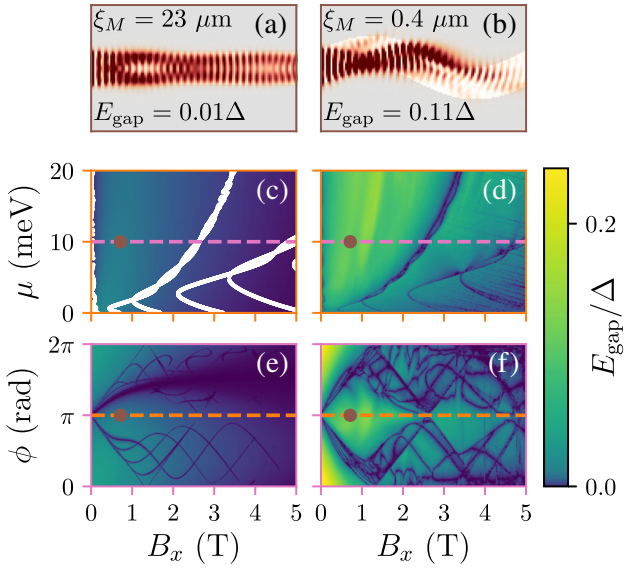

FIG. 4. A comparison of a straight device (left panels) and a zigzag one (right panels). The top panels show the Majorana wave functions, near the left edge of the system, at the value of B_x for which $E_{\rm gap}$ is maximized in a straight geometry for $\mu = 10$ meV and $\phi = \pi$ as well as the values of the gap and the Majorana size. The other panels show gap as a function of μ and B_x at $\phi = \pi$ (middle panels) and as a function of ϕ and B_x at $\mu = 10$ meV (bottom panels). The dashed lines and the dot indicate the parameters used in the other panels. Additionally, in subplot (c), we overlay the phase boundaries. The remaining parameter values are listed at the end of the Setup section, except with $a = 5$ nm and $L_{\rm SC} = 800$ nm.

Additionally, we plot the first 1300 nm (one zigzag period) of the wave functions [4(a) and 4(b)] at the optimal point in parameter space for the straight system. For the straight system, we calculate $E_{\rm gap}$ by performing a binary search in E for the energy at which the propagating modes start to appear [18]. Additionally, in Fig. 4(c), we plot the phase boundaries obtained by solving a generalized eigenvalue problem [18]. Because of the large size of the zigzag supercell, we are unable to apply these methods to zigzag geometries. Instead, we calculate $E_{\rm gap}$ by finding the absolute minimum of the spectrum $E_{\rm gap} = \min |E(k)|$. By both observing the gap closings and comparing to the topological phase diagram of the straight system, we then infer the topology of the zigzag system and verify this by calculating the Majorana wave function of a finite length zigzag. As a further check, in the Supplemental Material [23], we also compute $E_{\rm gap}$ as a function of the angle of magnetic field and observe that the zigzag device protects Majoranas from magnetic field misalignments.

Similar to the findings of Pientka *et al.* [12], we see that the straight geometry has a diamond-shaped topological region in (ϕ, B_x) space. The topological phase diagram of the zigzag system has a qualitatively similar shape but a significantly increased topological gap. The asymmetry of the phase diagram upon replacing $\phi \to -\phi$ is consistent with the symmetry of the Hamiltonian, because both inversion and time reversal change both $\phi \to -\phi$ and $B_x \to -B_x$.

Discussion and conclusions.—The zigzag geometry increases the topological gap in the high-density regime by more than an order of magnitude and substantially reduces Majorana size. The improvements occur in a broad range of parameter values, moreover, even using B_x optimal for the straight system in the high-density regime (Fig. 4), the Majorana size ξ_M and $E_{\rm gap}$ are still more than an order of magnitude better for the zigzag system. We expect that the improvement of the device performance will significantly simplify the creation of Majorana devices and the detection of Majorana states. Additionally, it offers a controllable way to remove long trajectories, making it easier to rely on than disorder [22], which has a similar effect.

A soft gap may arise due to mechanisms that do not involve ballistic trajectories: both interface disorder and pair breaking [27] or temperature and dissipation [28] may create a soft gap. Further, in a multimode junction, the dependence of transmission [29] may produce a subgap conductance similar to that in a device with a soft gap. The zigzag geometry has no impact on these alternative phenomena, and therefore, it may serve as a tool for distinguishing different mechanisms.

Our work is the first demonstration of the impact of the Majorana device geometry on its performance, and it opens a possible research avenue for finding the optimal geometry. A promising approach for tackling this question would rely on constructing a quasiclassical model of the zigzag devices. Finally, we neglected several important physical effects, such as disorder, electrostatics, the orbital effect of the magnetic field, and the finite thickness of the sample. Although we do not expect these phenomena to influence our qualitative findings, a more detailed simulation should provide better guidance to future experiments.

The zigzag geometry is within reach of the standard fabrication techniques as demonstrated by an ongoing experimental project [30]. Further, according to our simulations, the zigzag devices should be robust against the unavoidable variation in the experimental device geometry. Therefore, we expect that the new approach to controlling the proximity superconductivity by means of modifying the geometry will become a commonly used technique.

We are grateful to S. Goswami, A. Keselman, P. P. Piskunow, T. Ö. Rosdahl, D. Varjas, F. K. de Vries, Q. Wang, and J. B. Weston for useful discussions. This work was supported by the Netherlands Organization for Scientific Research (NWO/OCW), as part of the Frontiers of Nanoscience Program, two NWO VIDI grants (Grants No. 016.Vidi.189.180 and No. 680-47-537), an ERC Starting Grant No. STATOPINS 638760, and the project Quantox of QuantERA ERA-NET Cofund in

Quantum Technologies (Grant Agreement No. 731473) implemented within the European Union's Horizon 2020 Program. T. L. authored the idea of the zigzag geometry. B. N. wrote the code and it was extended by T. L. B. N. performed the writing of the manuscript with input of the other authors. All authors performed the analysis of the results and planning of the project.

*tlaeven@hotmail.com
†bas@nijho.lt
‡m.t.wimmer@tudelft.nl
§zigzag@antonakhmerov.org

[1] R. M. Lutchyn, J. D. Sau, and S. Das Sarma, Phys. Rev. Lett. **105**, 077001 (2010).
[2] Y. Oreg, G. Refael, and F. von Oppen, Phys. Rev. Lett. **105**, 177002 (2010).
[3] J. Alicea, Rep. Prog. Phys. **75**, 076501 (2012).
[4] C. Beenakker, Annu. Rev. Condens. Matter Phys. **4**, 113 (2013).
[5] C. Beenakker and L. Kouwenhoven, Nat. Phys. **12**, 618 (2016).
[6] M. Leijnse and K. Flensberg, Semicond. Sci. Technol. **27**, 124003 (2012).
[7] V. Mourik, K. Zuo, S. M. Frolov, S. R. Plissard, E. P. A. M. Bakkers, and L. P. Kouwenhoven, Science **336**, 1003 (2012).
[8] A. Das, Y. Ronen, Y. Most, Y. Oreg, M. Heiblum, and H. Shtrikman, Nat. Phys. **8**, 887 (2012).
[9] M. T. Deng, C. L. Yu, G. Y. Huang, M. Larsson, P. Caroff, and H. Q. Xu, Nano Lett. **12**, 6414 (2012).
[10] H. O. H. Churchill, V. Fatemi, K. Grove-Rasmussen, M. T. Deng, P. Caroff, H. Q. Xu, and C. M. Marcus, Phys. Rev. B **87**, 241401(R) (2013).
[11] H. Zhang *et al.*, Nature (London) **556**, 74 (2018).
[12] F. Pientka, A. Keselman, E. Berg, A. Yacoby, A. Stern, and B. I. Halperin, Phys. Rev. X **7**, 021032 (2017).
[13] M. Hell, M. Leijnse, and K. Flensberg, Phys. Rev. Lett. **118**, 107701 (2017).
[14] A. Fornieri, A. M. Whiticar, F. Setiawan, E. Portolés, A. C. C. Drachmann, A. Keselman, S. Gronin, C. Thomas, T. Wang, R. Kallaher, G. C. Gardner, E. Berg, M. J. Manfra, A. Stern, C. M. Marcus, and F. Nichele, Nature (London) **569**, 89 (2019).
[15] H. Ren, F. Pientka, S. Hart, A. T. Pierce, M. Kosowsky, L. Lunczer, R. Schlereth, B. Scharf, E. M. Hankiewicz, L. W. Molenkamp, B. I. Halperin, and A. Yacoby, Nature (London) **569**, 93 (2019).
[16] P. de Gennes and D. Saint-James, Phys. Lett. **4**, 151 (1963).
[17] C. Beenakker, in *Quantum Dots: A Doorway to Nanoscale Physics* (Springer, Berlin, Heidelberg, 2005), pp. 131–174.
[18] B. Nijholt and A. R. Akhmerov, Phys. Rev. B **93**, 235434 (2016).
[19] A. A. Golubov and M. Y. Kupriyanov, J. Low Temp. Phys. **70**, 83 (1988).
[20] W. Belzig, C. Bruder, and G. Schön, Phys. Rev. B **54**, 9443 (1996).
[21] S. Pilgram, W. Belzig, and C. Bruder, Phys. Rev. B **62**, 12462 (2000).
[22] A. Haim and A. Stern, Phys. Rev. Lett. **122**, 126801 (2019).
[23] See Supplemental Material at http://link.aps.org/supplemental/10.1103/PhysRevLett.125.086802 for additional study of the robustness of zigzag devices, as well as a comparison between having a rough NS interface and a full zigzag, to demonstrate the gap improvement is derived from cutting off long trajectories. The zigzag concept is also demonstrated for systems with a single NS junction.
[24] C. W. Groth, M. Wimmer, A. R. Akhmerov, and X. Waintal, New J. Phys. **16**, 063065 (2014).
[25] B. Nijholt, J. Weston, J. Hoofwijk, and A. Akhmerov, Adaptive: parallel active learning of mathematical functions (2019), http://doi.org/10.5281/zenodo.1182437.
[26] T. Laeven, B. Nijholt, A. R. Akhmerov, and M. Wimmer, Enhanced proximity effect in zigzag-shaped Majorana Josephson junctions (2019), http://doi.org/10.5281/zenodo.2578027.
[27] S. Takei, B. M. Fregoso, H.-Y. Hui, A. M. Lobos, and S. Das Sarma, Phys. Rev. Lett. **110**, 186803 (2013).
[28] C.-X. Liu, F. Setiawan, J. D. Sau, and S. Das Sarma, Phys. Rev. B **96**, 054520 (2017).
[29] T. D. Stanescu, R. M. Lutchyn, and S. Das Sarma, Phys. Rev. B **90**, 085302 (2014).
[30] F. K. de Vries, Q. Wang, and S. Goswami (private communication).